Improved ultraviolet stability of fullerene-based organic solar cells through light-induced enlargement and crystallization of fullerene domains

Elena Barulina, Anass Khodr, Sadok Ben Dkhil, Pavlo Perkhun, Yatzil Alejandra Avalos Quiroz, Tomoyuki Koganezawa, Noriyuki Yoshimoto, Wolfgang Köntges, Rasmus Schröder, Martin Pfammöller, et al.

Improved ultraviolet stability of fullerene-based organic solar cells through light-induced enlargement and crystallization of fullerene domains.

Elena Barulina,[1,2] Anass Khodr,[1,2] Sadok Ben Dkhil,[2] Pavlo Perkhun,[1] Yatzil Alejandra Avalos Quiroz,[1] Tomoyuki Koganezawa,[3] Noriyuki Yoshimoto,[4] Wolfgang Köntges,[5] Rasmus R. Schröder,[5] Martin Pfammöller,[5] Olivier Margeat,[1] Jörg Ackermann,[1] Christine Videlot-Ackermann,[1,]*

[1] Aix Marseille Univ., UMR CNRS 7325, CINaM, 13288 Marseille, France.

[2] Dracula Technologies, 3 rue Georges Auric, 26000 Valence, France.

[3] Industrial Application Division, Japan Synchrotron Radiation Research Institute (JASRI), Sayo, Hyogo 679-5198, Japan.

[4] Department of Physical Science and Materials Engineering, Iwate University, Ueda Morioka 020 8551, Japan.

[5] CAM, Centre for Advanced Materials, Heidelberg University, Heidelberg, Germany.

ABSTRACT

Organic solar cells (OSCs) are a promising technology with the potential for low-cost manufacturing. However, to translate to economically viable applications, long-term stability is a fundamental requirement. Amongst intrinsic degradation pathways the sensitivity of OSC to ultraviolet (UV) light severely limits their photostability. Here, we focus on the impact of UV on the stability of solar cells based on well-known fullerene-based blends processed with 1,8-diidooctane (DIO) as additive. The post-annealed devices resulting in DIO-free blends are directly compared to as-cast devices containing residual DIO. After a pronounced initial burn-in, as-cast devices demonstrate a self-healing effect leading to stable solar cells under prolonged exposure to UV light. This initial burn-in can be considerably reduced in annealed devices with a

suitable heating process, resulting in very stable solar cells under UV-containing light over a long time period. Under UV-free LED light, solar cells are stable, which implies a direct impact of UV on the performance evolution of devices. Advanced characterization techniques were used for in-depth morphological analyses under light exposure to distinguish the observed UV-related processes in the polymer blends. Our results point thus towards the presence of two processes occurring under UV-light within as-cast devices involving fullerenes, one causing a performance degradation and the other allowing a repair tending towards a performance stability. Due to an improved initial crystal order within annealed devices, the process related to the degradation is in the minority. The UV stability of devices can be attributed to the UV light-induced diffusion of fullerenes, leading jointly to the enlargement of the initial existing fullerene domains and to their crystallization under UV light. These results path the way for a better understanding of the stability of efficient normal OSCs under simulated sunlight.

KEYWORDS: Polymer solar cells; Fullerene; 1,8-diiodooctane; Normal structure; Morphology; Photostability; Ultraviolet light.

1. INTRODUCTION

Nowadays organic solar cells (OSCs) are very attractive emerging photovoltaic technology due to their low-cost printing production, low energy payback time and improvement in efficiency up to 18% in single junction [1-3]. The most efficient solution-processable organic solar cells are based on bulk heterojunction (BHJ) blends of an electron donating conjugated polymer (p-type semiconductor) and a n-type material usually represented by fullerene derivatives or non-fullerene acceptors (NFAs) [1,3,4-6]. Since the performance of OSCs is now suitable for commercial applications, focus should be placed on operational stability studies as high

efficiency and device stability must be combined for commercialization [7]. However, the amount of research devoted to the development of materials to improve the power conversion efficiency (PCE) is still high compared to the work on the study of stability [8-14]. As OSCs are multi-layered stacks, several degradation mechanisms can occur, including chemical reactions induced by light, oxygen and water in the active layer, device electrodes and charge extraction layers [15,16]. Among these factors, the interaction of OSCs with ultraviolet (UV)-light is one of the critical degradation factors, which makes it necessary to use a specific UV filter to improve their lifetime [17-20]. The identification of material and device structure strategies that enable the generation of OSCs with improved UV-light stability is an interesting approach to promote future commercial applications of OSCs. In the past, several studies have investigated the stability of OSC devices using fullerene and NFAs, respectively, under unfiltered-UV sunlight conditions [10,21-29]. For instants, UV instabilities of solar cells using [6,6]-Phenyl-C71-butyric acid methyl ester ($PC_{71}BM$) and NFAs based blends toward the processing additive 1,8-diiodooctane (DIO) have been demonstrated [21,25-28]. A photochemical reaction product of $PC_{71}BM$ with UV-induced radicals of DIO was identified as the cause of the device degradation [25]. To improve the stability of the device under unfiltered UV light, replacing DIO with a UV-absorbing additive, benzophenone, proved to be a promising approach [26]. It was also found that thermal annealing of the fullerene-based solar cells at 85°C clearly improved the stability of the device under UV-light by improving the crystal order in the acceptor domains [21]. The majority of studies that perform stability measurements use inverted device structures, only a few studies address device stability using normal device structures [26,27]. Interestingly solar cells based on $PC_{71}BM$ blended with poly([2,6′-4,8-di(5-ethylhexylthienyl)benzo[1,2-b;3,3-b]dithiophene]{3-fluoro-2[(2-ethylhexyl)carbonyl]thieno[3,4-b]thiophenediyl}) (PTB7-Th) and DIO using a normal device structure showed improved stability under unfiltered-UV simulated sunlight compared to inverted devices [27].

In this work, we focus on the normal device structure in combination with the use of DIO as additive and thermal treatment to improve and understand the UV stability of OSCs. We selected blends based on $PC_{71}BM$ and PTB7-Th (Figure 1a) processed with DIO as photoactive layers. In addition to the inclusion of an additive, a specific two-steps thermal post-treatment on complete devices was used to study the impact of enhanced crystalline order in the polymer blend on the UV stability of the solar cells. The annealing procedure consists of a high temperature step at 140°C for 10 min followed by a second annealing step at 85°C for 1 h. This post-annealing procedure containing a step at 140°C is named here PAS-140. As-cast devices, *i.e.* not heat-treated, were used as a reference. Light soaking experiments were performed with either UV-containing simulated AM1.5 light using a Xenon lamp or UV-free LED light (Figure 1b). Before light soaking for the lifetime study, the devices were encapsulated to protect them from air degradation (Figure 1c). Our results reveal that there is a marked difference in the degradation rate and overall stability of the device under UV-light exposure. While as-cast devices demonstrate a self-healing effect after a pronounced initial burn-in which leads to stable solar cells under UV-containing light soaking, this initial burn-in can be considerably reduced for PAS-140 devices, resulting in very stable solar cells under UV-containing light for 250 hours. On the contrary, under UV-free LED light, solar cells are stable. The two surface analysis techniques, atomic force microscopy (AFM) and contact water angle (CWA) measurement, reveal a UV-induced migration of fullerene molecules towards the top surface. To understand the UV related performance modification in volume, the structure and morphology of blend layers have been studied before and after light soaking with analytical transmission electron microscopy (ATEM) and 2D grazing-incidence X-ray diffractometry (2D-GIXRD). ATEM analyses reveal UV-induced fullerene diffusion within the mixture, which leads to an increase in the size of the $PC_{71}BM$ domains. Furthermore, 2D-GIXRD analysis highlight a UV-induced crystallinity inside $PC_{71}BM$ domains. Importantly, under UV-free light, the morphology of the

blends remained unchanged compared to non-exposed light cells. These results suggest that the difference in UV stability of devices may be due to UV light-induced diffusion of the fullerenes, leading jointly to the enlargement of the initial existing fullerene domains and to their crystallization under UV.

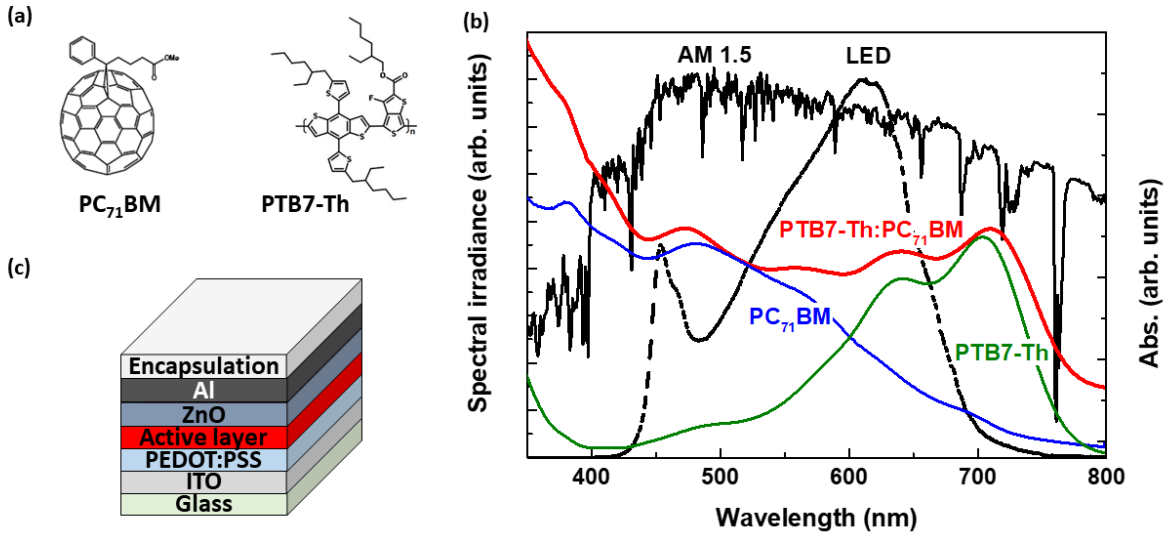

Figure 1. (a) Chemical structure of $PC_{71}BM$ and PTB7-Th. (b) Comparison between spectrum of LED lamp and standard sunlight at AM 1.5 together with the absorption spectra of $PC_{71}BM$, PTB7-Th and PTB7-Th:$PC_{71}BM$ bulk heterojunction films. (c) Normal structure employed in bulk heterojunction organic solar cells.

2. EXPERIMENTAL METHOD

2.1 Materials: PTB7-Th and $PC_{71}BM$ (95% purity) were purchased from 1-Material and Nano-C, respectively (Figure 1a). Poly(2,3-dihydrothieno-1,4-dioxin)-poly(styrenesulfonate) (PEDOT:PSS at 95%) was purchased form Clevious Al 4083 and indium tin oxide (ITO) coated glass slide from Lumtec (15 ohm/sq). Chlorobenzene CB (anhydrous, 99.8%), DIO (98%, contains copper as stabilizer), ethanolamine EA (98%) and isopropanol (anhydrous, 99.5%) were purchased from Sigma Aldrich. Zinc oxide (ZnO) nanoparticle inks were prepared as published

elsewhere [30]. All commercial materials were used as received without purification and kept under argon atmosphere. Epoxy glue Katiobond LP 655 was purchased from DELO and kept in a refrigerator.

2.2 Fabrication and characterization of solar cells: The solar cells were fabricated in normal structure (ITO/PEDOT:PSS/PTB7-Th:$PC_{71}BM$/ZnO/Al) on ITO-coated glass substrates using spin-coating technique in glove box under controlled argon atmosphere (Figure 1c). Glass substrates with ITO patterned layers were cleaned in ultrasonic bath successively in water, acetone, ethanol and isopropanol during 10 min. The substrates were treated to ultraviolet-ozone during 15 min at 80°C. A thin layer of PEDOT:PSS as hole transporting layer with thickness of 40 nm was spin-coated on cleaned glass substrate at 3500 rpm during 60 sec, following by an annealing step at 140°C for 15 min. The mixture of PTB7-Th:$PC_{71}BM$ was prepared with a ratio 1:2 with a donor concentration of 10 mg/ml and 3 vol% of DIO was added after 1 h of stirring of donor and acceptor mixture in chlorobenzene at 65°C. The final mixture was stirred overnight. Thin films were deposited at 2500 rpm during 120 sec (thickness 114±3 nm) with subsequent drying in high vacuum overnight. ZnO was dissolved in 5 mg/ml in isopropanol with 0.1 vol. % of EA. ZnO solution was spin-coated at 1500 rpm and annealed at 80°C in glove box to form the electron transporting layer. Aluminium (Al) electrode was then thermally evaporated at 1.3×10^{-4} Pa with a thickness of 100 nm using a shadow mask for a solar cell area to 0.27 cm^2.

The post-annealing treatment (named PAS-140) was applied in glove-box on complete devices at 140°C during 10 min following by a second annealing step at 85°C during 1 h [31]. The devices were encapsulated in glove box by the application of solvent-free ultraviolet epoxy DELO Katiobond LP 655 glue followed by the deposition of a pre-cleaned and ultraviolet-ozone pre-treated glass for 15 min at 80°C on the top. In order to prevent penetration from the sides of the stack (which is often accelerated by water-soluble layers like PEDOT:PSS) of air contaminants,

the sides of the component have been cleaned in order to remove the PEDOT:PSS, ZnO and BHJ layers. DELO Katiobond LP 655 glue is a light-UV-curing adhesive with high barrier function against water vapor. Encapsulated devices were exposed to 1-Sun illumination (100 mW/cm^2, AM1.5) during 10 min and kept during night in glove box to complete the polymerization.

The current density-voltage (J-V) measurements were done inside the glove box using a Keithley 238 Source Measure Unit and a Newport class AAA Global solar simulator (Oriel Sol3ATM model no. 94043A) with light intensity of 100 mW/cm^2. The light intensity was determined with a silicon reference cell from Newport Company, Oriel no.94043A calibrated by National Renewable Energy Laboratory.

The continuous long stability was measured outside of the glove box in a Candlelight system with periodically saving maximum power point (MPP) and J-V curves under white LED and under AM1.5G Solar 1A Oriel with intensity of 100 mW/cm^2 using a register system (see spectra in Figure 1b). For both light sources, the illumination has been realized through ITO substrates. To monitor the photodegradation of the devices over time, J-V curves were collected every hour, while the devices were kept at open circuit conditions during light soaking. During the recording of the experiment, the temperature of the cells was controlled and kept below 40°C. LED light was calibrated by matching the device current to those measured under AM1.5G with an UV filter below 400 nm with the intensity 100 mW/cm^2 and the source-meter. The devices were kept at MPP tracking with tracking step 0.33 mV.

2.3 Characterization of thin films: The thicknesses of the layers were measured by a profilometer Dektak XTS (Bruker, Germany) equipped with a stylus with radius 2 micron. The absorption of the thin films was measured by the Spectrometer Cary 5000. Contact water angle (CWA) measurements were performed by video-based optical contact angle measuring by static mode by OCA 20 instrument from DataPhysics Instrument GmbH Company in a room with a

controlled temperature at 20ºC. The surface morphology of the layers processed on PEDOT:PSS was studied by atomic force microscopy (AFM) using a Nanoscope III in the taping mode.

Thin films were further analyzed by 2D-GIXRD)with high-brightness synchrotron radiation at BL19B2 in SPring-8 (Japan). 2D-GIXRD measurements were performed using a high-sensitive 2D X-ray detector (PILATUS 300K). The incident angle and wavelength of X-rays were 0.13° and 0.100 nm, respectively. The crystal coherence length (CCL) values were extracted by the Scherrer equation from full width at half maximum (FWHM):

$$\tau = \frac{K\lambda}{\beta\cos\theta} \quad (1)$$

where $\boldsymbol{\tau}$ is the ordered (crystalline) domains mean size, here defined as CCL, **K** is a constant (dimensionless shape factor) closed to unity. The shape factor is typically equal to 0.9, $\boldsymbol{\lambda}$ is the wavelength of the X-ray, $\boldsymbol{\beta}$ is the FWHM of the diffraction peak in radians after subtracting the instrumental line broadening and $\boldsymbol{\theta}$ is the Bragg angle.

Thinner layers based on PTB7-Th:$PC_{71}BM$ blends with a nominal thickness of 40 nm were prepared by spin-coating at 12000 rpm for 1 min for analytical transmission electron microscopy (ATEM). The photoactive layers processed on ITO substrates covered by PEDOT:PSS were post-annealed with PAS-140 before floated upon demineralized water and collected with holey carbon grids (QUANTIFOIL). Transmission electron microscopy (TEM) measurements were performed with a Cs aberration corrected Libra 200 MC Cryo DMU (Carl Zeiss Microscopy GmbH, Germany) at 60 kV equipped with a corrected in-column energy filter and a monochromator. Electron energy loss (EEL) spectra were recorded from pure and blend layers with an energy resolution of 85 meV. Electron spectroscopic images (ESI) series were recorded using a slit aperture of 1 eV in the energy dispersive plane of the microscope from 5 to 45 eV. For acquisition of a whole series, a total dose of 55000 e/$Å^2$ was applied. Various image-preprocessing steps for denoising by thresholding and Fourier filters on all images were applied using self-written scripts in python in combination with the open source software ImageJ (NIH).

Image registration and nonlinear multivariate analyses (locally linear embedding) of the ESI stacks were performed using ITK [32] and Ilastik [33], respectively as described elsewhere [34,35]. Locally linear embedding is also implemented in other well-known software packages such as Matlab (MathWorks, USA) or Python with the scikit-learn package. A random forest classifier was trained on label subsets for classification of all remaining pixels resulting into material distribution maps. Layer thickness in the TEM was measured by applying the Fourier-log-ratio-method [36]. Several ESI stacks were acquired from six PTB7-Th:$PC_{71}BM$ blends in total.

3. RESULTS AND DISCUSSION

3.1 Impact of UV-light soaking on solar cells performances

BHJs were realized by mixing PTB7-Th and $PC_{71}BM$ with a 1:2 weight ratio in CB as deposition solvent and 3 vol% of DIO as solvent additive. In order to remove the solvent molecules after spin-coating process, we applied a high-vacuum drying step (1.3×10^{-6} Pa) followed by a post-annealing treatment. Indeed, while the CB dispersion solvent (a low boiling solvent, T_b = 132°C) is mainly eliminated during the vacuum phase, residual DIO molecules (a high boiling point additive T_b = 167-169°C) remain in the blend in trace amounts despite this high vacuum drying process [37,38]. A post-deposition treatment as post-annealing is therefore necessary to achieve the BHJ's drying process and its reorganization [39]. A previous study demonstrated that a specific two-stage thermal annealing process, named PAS-140, was able to remove residual DIO in the blend layers, in addition to the conventional vacuum drying step applied to polymer blends during device processing [40]. PAS-140, consisting of a step at 140°C for 10 min followed by 85°C for 1 h, was applied to the blend-based thin films without affecting the absorption spectra (not shown here).

Light soaking experiments were performed with either a UV-containing simulated AM1.5 light using a Xenon lamp or a white UV-free LED light, respectively. The emission spectra of LED and AM1.5 lights are shown in Figure 1b together with the absorption spectra of pure compounds, $PC_{71}BM$ and PTB7-Th, and PTB7-Th:$PC_{71}BM$ blended films. Importantly, the LED light is free of UV wavelength, while the emission spectrum of the Xenon lamp contains both UV and visible wavelengths. Comparison of the emission spectra of the two lamps with the absorption spectra of the films reveals that, depending on the light source, the absorption of the light within the blend will be very different. While $PC_{71}BM$ shows strong light absorption in the UV range with a continuously decrease up to 700 nm in the visible, PTB7-Th absorption is located in the visible region from 500 to 800 nm. The absorption spectrum of the PTB7-Th:$PC_{71}BM$ blend corresponds well to the addition of the two spectra of the single layers and covers the entire visible absorption range. Thus under AM1.5 light, the fullerenes are strongly exposed to UV-light when not under LED. PTB7-Th will also be much less affected by LED exposure with a light excitation up to 700 nm reducing the impact on the photodegradation process. While LED are not expected to have an impact on the photodegradation process of the BHJ films, the presence of UV-light in the AM1.5 spectrum should have a strong impact on blends and in particular on fullerenes.

To study the impact of light soaking on device performances, encapsulated solar cells in normal structure were exposed to UV-containing AM1.5 light. As-cast and PAS-140 post-annealed solar cells have been studied in the same conditions. Table 1 shows the initial photovoltaic parameters of fresh solar cells as power conversion efficiency PCE, open-circuit voltage V_{oc}, short-circuit density J_{sc} and fill factor FF. Time profiles of photovoltaic parameters upon ageing under UV-containing AM1.5 illumination are shown in Figure 2. As-cast devices show an unexpected behavior for PCE with an initial long burn-in of 70 h (zone I) following by a gradual and slow self-healing effect (zone II) in order to achieve stable solar cells under UV-light soaking. The

same evolution is observed in FF, which highlights a potential morphological evolution of the layer during light soaking. Remarkably, the initial burn-in can be significantly reduced for PAS-140 post-annealed devices. Despite a reduction in the initial PCE value by thermal annealing, as previously shown in the work of Liu *et al.* mainly generated by FF losses [21], an inherently improved stability to UV-light with PAS-140 is substantially achieved with only 0.5% loss over 250 h, which corresponds to an unpreceded calculated T_{80} (time during which the efficiency decreases to 80% of its initial value) of 2800 h. We also evaluated the stability of the devices under UV-free light, as shown in Figure 3, where the solar cells are extremely stable and free of any initial burn-in. Therefore, the observed difference in stability under UV-containing and UV-free light soaking is exclusively caused by exposure to UV wavelengths.

Table 1: Initial photovoltaic parameters (J_{sc} V_{oc}, FF and PCE) of fresh encapsulated solar cells.

Condition	Jsc (mA/cm^2)	V_{oc} (V)	FF (%)	PCE (%)	PCE_{av}[(a)] (%)
as-cast	16.9	0.80	61	8.1	7.6[(3)]
PAS-140	16.8	0.82	54	7.4	7.15[(8)]

[(a)] n is the number of cells to provide an average PCE ($PCE_{av.}$)

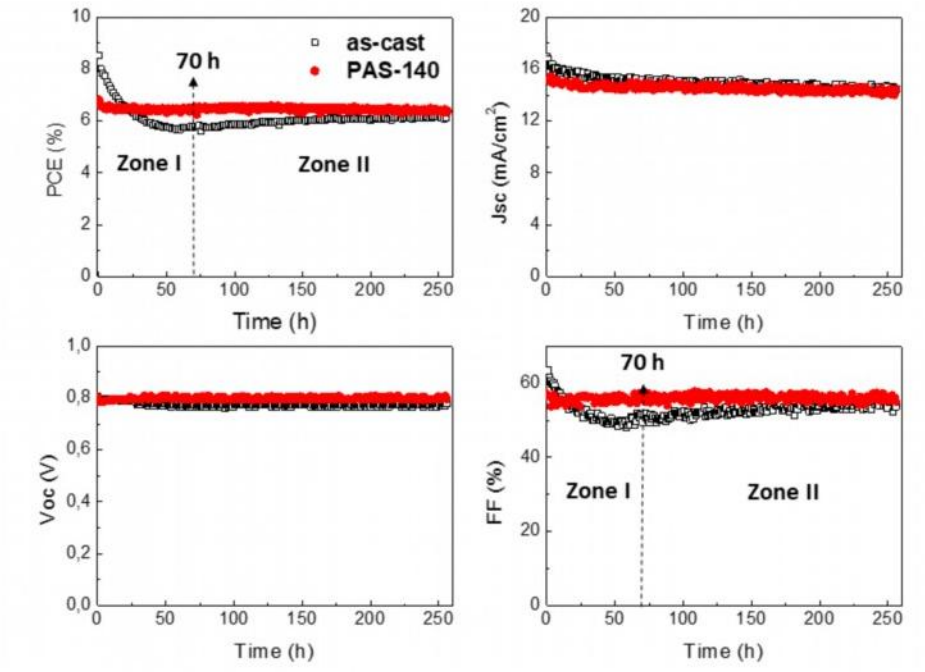

Figure 2. PCE, J_{sc}, V_{oc} and FF as a function of illumination time for encapsulated solar cells based on as-cast or PAS-140 post-annealed PTB7-Th:$PC_{71}BM$ bulk heterojunction blends. Illumination was realized in air at 1 sun (100 mW/cm^2, UV-containing simulated AM1.5 light).

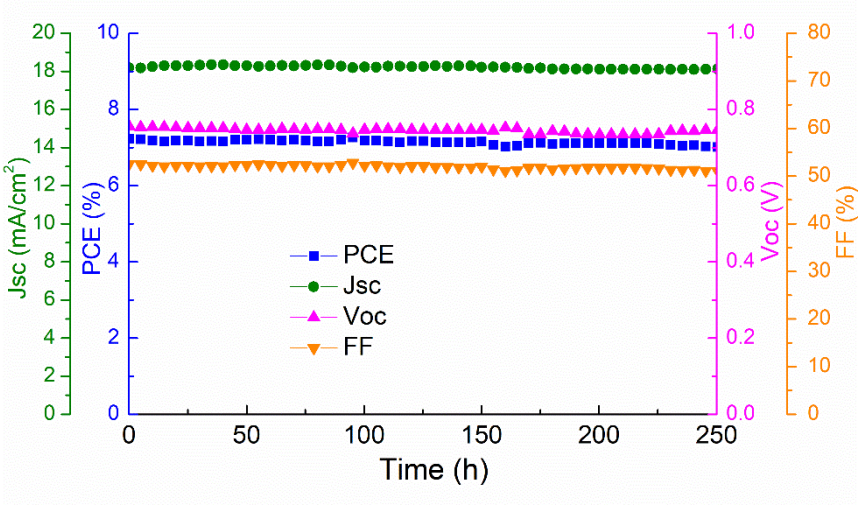

Figure 3. PCE, J_{sc}, V_{oc} and FF as a function of illumination time for encapsulated solar cells based on PAS-140 annealed PTB7-Th:$PC_{71}BM$ bulk heterojunction blends. Illumination was realized in air under LED.

3.1 Impact of UV-light soaking on thin film morphology

3.1.1 Surface analysis

Figure 4 shows AFM phase images of as-cast and PAS-140 post-annealed PTB7-Th:$PC_{71}BM$ blends. Thin films were exposed individually to UV-free LED or UV-containing simulated AM1.5 lights in inert atmosphere. The illumination times (> 70 hours) were deliberately chosen in zone II corresponding to the self-healing phase of the as-cast cells (see Figure 2). Films stored in the dark are used as reference (storage time 100 hours). The surface morphology of both as-cast and post-annealed polymer blends is unchanged at the initial observation under both illuminations, only the root mean square roughness (rms) shows slight differences. A comparable value is noted between LED and dark with values of 1.4-1.5 nm signifying an identical surface state. On the contrary, a change is induced by UV-containing light where smaller rms of 1.1-1.2

nm are measured. To provide information on the wettability evolution of the surface components of blend films, we realized WCA characterization on blends under different conditions (Figure 5) [41]. The WCAs of pure PTB7-Th and $PC_{71}BM$ films stored in dark were 95.5° and 79.2°, respectively, indicating that $PC_{71}BM$ has a relatively strong hydrophilic property [42]. For PAS-140 post-annealed PTB7-Th:$PC_{71}BM$ blends, as expected, the WCA in dark is slightly less (93.6°) than pure PTB7-Th films due to the appearance of $PC_{71}BM$ on the top surface of blend films. Under AM1.5 illumination, this WCA will decrease slightly to reach 92.5° displaying a weak vertical segregation of fullerenes towards the blend surface. The same tendency has been observed for as-cast PTB7-Th:$PC_{71}BM$ blends. This UV-induced migration of fullerene molecules can also explain the lower surface roughness measured under UV-containing simulated AM1.5 light.

Both AFM and WCA as surface analysis techniques will not reveal whether these changes are also present in the volume. It is therefore necessary to use other analytical techniques to probe the volume structural state of the blends.

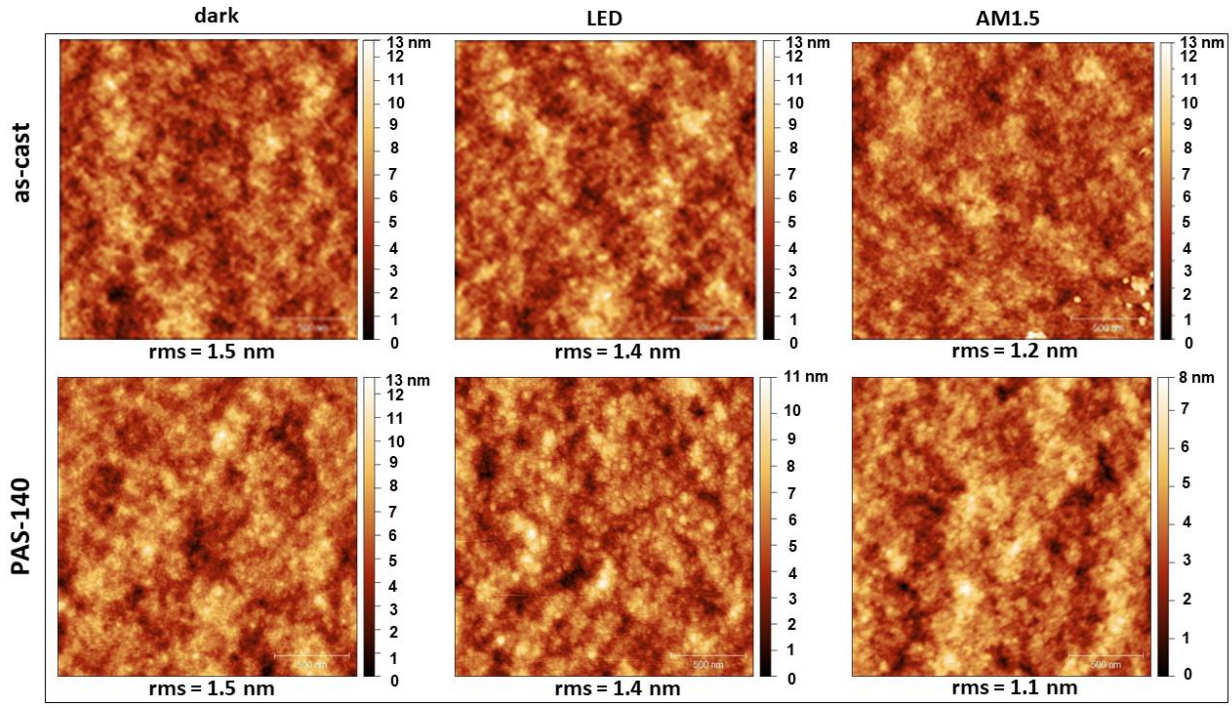

Figure 4. Atomic force microscopy phase images of as-cast and PAS-140 post-annealed PTB7-Th:$PC_{71}BM$ bulk heterojunction blends: stored in dark or exposed individually to LED light

during 160 hours or 1 sun illumination (UV-containing simulated AM1.5 light) during 100 hours. Exposition to light sources or dark storage were realized in glove-box. Scale: 2×2 μm^2.

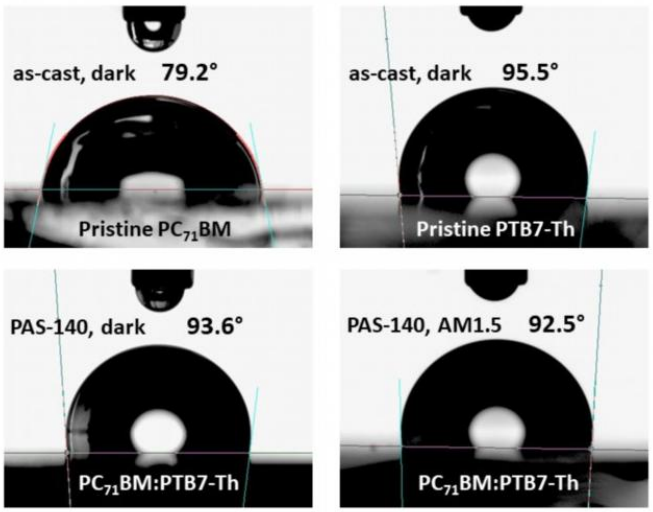

Figure 5. Water contact angle images of the top surface of as-cast $PC_{71}BM$ and PTB7-Th films together with PAS-140 post-annealed $PC_{71}BM$:PTB7-Th blends stored in dark or exposed under a prolonged UV-containing simulated AM1.5 illumination of 70 h.

3.1.2 Bulk analysis

The UV-light induced morphological changes were further studied by ATEM measurements on as-cast and PAS-140 post-annealed PTB7-Th:$PC_{71}BM$ blends before and after illumination with UV-containing AM1.5 light. ATEM technique allows studying not only the top surface of the layer but more particularly the morphology of the underlying layers. ATEM combines EEL spectroscopy with ESI and has been proven to reliably visualize the material phase distribution of fullerene and more recently non fullerene based blends [34,35]. The analysis of EEL spectra from pure PTB7-Th and $PC_{71}BM$ films as well as the analysis of ESI stacks from PTB7-Th:$PC_{71}BM$ blends for segmenting material phases are provided in Figure 6. Blends proceed with 3 vol% of DIO as additive were analyzed as (i) as-cast films or (ii) PAS-140 post-annealed before and after a continuous UV-containing simulated AM1.5 light during 70 h. This aging time

under illumination of the cells corresponds to the transition time between zone I and zone II in Figure 2. The resulting material distribution maps is depicted in Figure 7. Red color corresponds to $PC_{71}BM$ enriched domains and blue color indicates PTB7-Th enriched domains, while mixed phases are marked in white. As an initial observation in Figure 7a, the size of fullerene-enriched domains increases after AM1.5 illumination. Figure 7b allows a finer analysis with corresponding histograms of particle size distribution curves of fullerene-enriched phases. By comparing the histograms before illumination, the frequency of small domains decreases for PAS-140 post-annealed blends with the appearance of domains larger than 20 nm. Continuous AM1.5 illumination of both layers also has the effect of promoting larger domains (> 25 nm) (see inserts in Figure 7b). These results clearly indicate that morphological changes in the volume of the blend upon demixing of fullerenes leading to larger fullerene domains are generated by annealing of the layers, but mostly by UV-light.

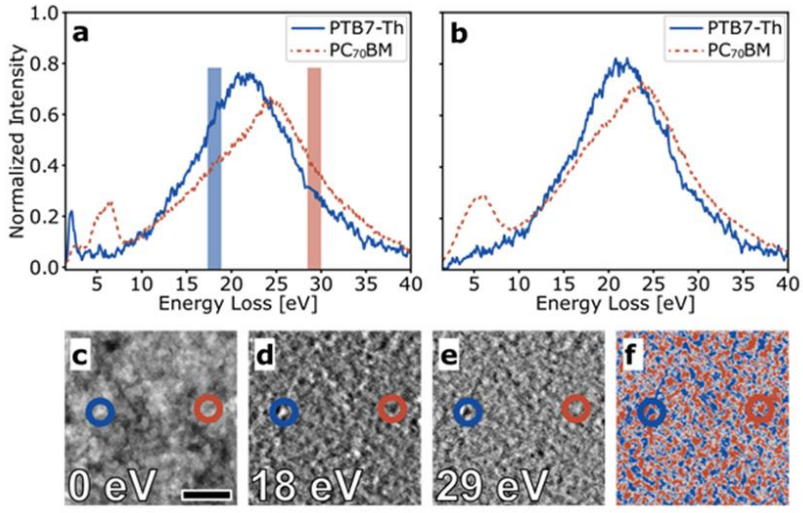

Figure 6: ATEM analysis of 40 nm thick PTB7-Th:$PC_{71}BM$ blend layers. **a.** EEL spectra of pure 40 nm thick PTB7-Th and $PC_{71}BM$ layers. The energy loss values 18 eV and 29 eV are highlighted by blue and red rectangles, respectively, at which the ESI images in (d) and (e) were acquired. **b.** EEL spectra of the same sample position as in (a) after a total dose of 8500e/$Å^2$ showing structural changes below 10 eV while the signals above show only minor changes. **c.** Zero loss image showing mass and density contrast of a 40 nm thick PTB7-Th:$PC_{71}BM$ blend

layer at same sample position as the ESI images taken at (d) 18 eV and (e) 29 eV. **d-e.** ESI images taken at the energy loss values indicated in (a) by blue and red rectangles showing inverted contrast. The contrast from mass and density variations have been compensated by normalizing the images by the sum of a whole ESI series from 5 eV to 45 eV. Blue and red circles mark positions of donor- and acceptor phases, respectively, assigned from the signal differences. **f.** Material distribution map determined by multivariate statistical analysis and spectral classification from an ESI stack with images from 5-45 eV, including the images in (d) and (e). Scale bar represents 100 nm.

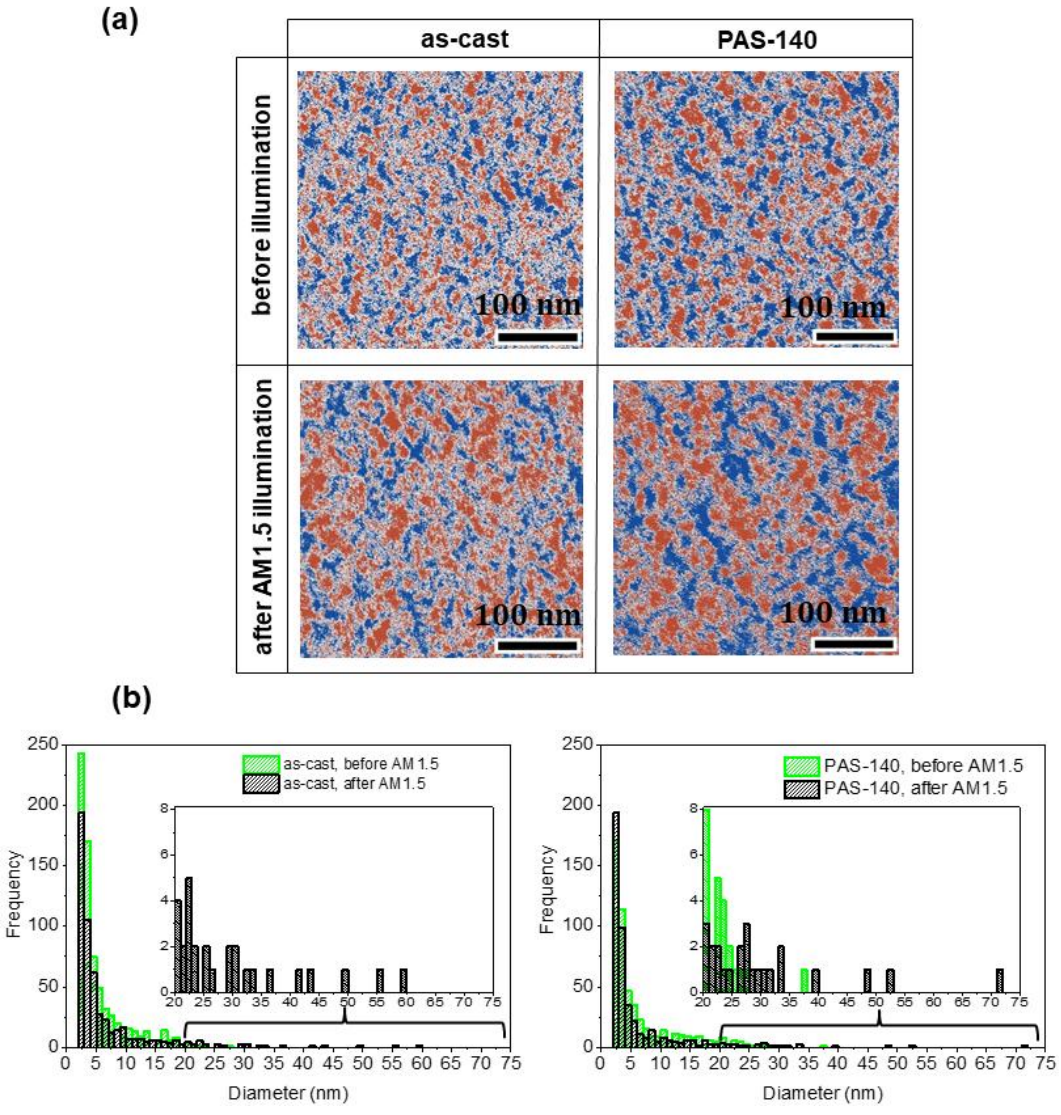

Figure 7: (a) ATEM images of PTB7-Th:$PC_{71}BM$ thin films before and after a continuous UV-containing simulated AM1.5 light during 70 h. Blends are as-cast or PAS-140 post-annealed. (b)

Histograms of particle size distribution curves of fullerene-enriched phases. Insert: zoom on the 20-75 nm diameter range.

To check if the UV-light-induced demixing stage is accompanied by a crystallization phase in the fullerene domains, we performed 2D-GIXRD measurements on PAS-140 post-annealed PTB7-Th:$PC_{71}BM$ blends. We probe molecular orientation, intermolecular distances and CCL in blends as a function of the light source, *i.e.* UV-containing simulated AM1.5 and UV-free LED. All films were processed under identical conditions and temperatures were maintained below 40°C for the duration of the light exposure under inert atmosphere. Figure 8 shows the 2D-patterns together with in-plane and out-of-plane GIXRD profiles of PTB7-Th:$PC_{71}BM$ blend films stored in dark or exposed individually to UV-free LED or UV-containing simulated AM1.5 light sources under inert atmosphere. While the in-plane profiles correspond to the addition of $PC_{71}BM$ and PTB7-Th peaks, the preservation of the (100) peak position at 0.29 $Å^{-1}$ corresponding to the lamellar *d*-spacing of PTB7-Th (d_{100} = 2.16 nm) indicates constant molecular orientation and intermolecular distances of polymer chains independently of light sources. For $PC_{71}BM$, a broad halo at 1.3 $Å^{-1}$ is observed indicating that $PC_{71}BM$ is amorphous [18]. We then extracted CCL values for both PTB7-Th and $PC_{71}BM$ compounds in the in-plane GIXRD profiles by the Scherrer equation (equation 1) from FWHM (Table 2). While CCL decreases slightly for PTB7-Th between dark storage to light soaking, a more significant increase is observed for $PC_{71}BM$ highlighting an increase in acceptor domain crystallinity under UV light. The most striking effect as function of light source is a strong change in the profile of the broad peak around 1.3 $Å^{-1}$ in the in-plane and out-of-plane GIXRD profiles of blends exposed to AM1.5 light. To gain better insight in the light induced changes, the dark profile of PTB7-Th:$PC_{71}BM$ blends was subtracted from those exposed to LED and AM1.5, respectively, and the resulting corrected profiles were compared to bare $PC_{71}BM$ profile as shown on the right side of Figure 8. With the persistence of peaks corresponding to $PC_{71}BM$ after the subtraction of

AM1.5 *vs* dark, this reveals that AM1.5 exposed layers exhibit strongly enhanced fullerene crystallinity compared to layers stored in dark or exposed to LED. The results clearly prove that UV-light introduces changes in the morphology of blends with light-induced crystallization of fullerene domains, while UV-free LED has no effect in the ordering of the blend. Importantly, the temperature of the blend films has been maintained to 35-40°C for both light sources excluding thus potential temperature related increase in fullerene order within the blend as a fullerene crystallization can be expected to proceed at temperatures higher than 110°C [43,44]. Taking into account that those layers were post-annealed with PAS-140 which removes DIO and generally stabilizes the blend morphology, we conclude that UV-light is an additional driving force to reorganize fullerenes in the blend morphology into ordered assemblies. The ordering of $PC_{71}BM$ was also observed recently through the formation of $PC_{71}BM$ aggregation in PTB7-Th:$PC_{71}BM$ films during UV-light soaking, while such clusters are not generated when a UV filter has been used [20].

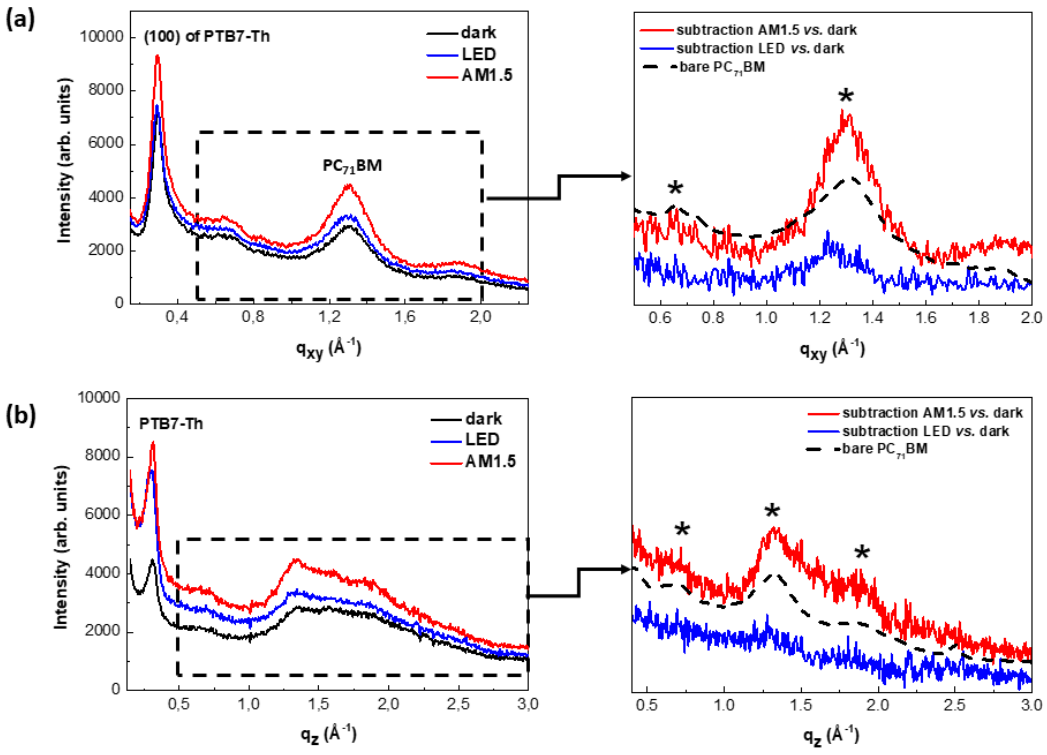

Figure 8. 2D-GIXRD profiles in plane (q_{xy}) (a) and out of plane (q_z) (b) of line cuts of PAS-140 post-annealed PTB7-Th:$PC_{71}BM$ bulk heterojunction blends conserved in dark or exposed to LED light (160 hours) or under 1 sun illumination (UV-containing simulated AM1.5 light, 100 hours). Exposition to light sources or dark storage were realized in glove-box. Right side: Dark profiles were subtracted to LED and AM1.5 profiles (named subtraction LED and subtraction AM1.5) and compared to bare $PC_{71}BM$ profile with identified peaks by a star.

Table 2: Full width at half maximum (FWHM) of diffraction peaks in the in-plane GIXRD profiles of PTB7-Th:$PC_{71}BM$ films together with crystal coherence length (CCL).

peak		FWHM	CCL (nm)
PTB7-Th (100) in plane (xy) at 0.29 $Å^{-1}$	dark	0.66	7.81
	LED	0.69	7.50
	AM1.5	0.68	7.63
$PC_{71}BM$ in plane (xy) at 1.3 $Å^{-1}$	**dark**	2.118	**4.35**
	LED	2.117	4.57
	AM1.5	2.100	**5.04**

3.3 Discussion

The stability of devices under simulated UV-containing sunlight, studied here in normal fullerene-based solar cells, showed an unprecedented evolution where self-healing or direct stabilization is observed instead of a common UV-light induced degradation. Since this particular self-healing of as-cast blends is absent under LED, our results suggest that this phenomenon is directly related to UV light exposure. Furthermore, as the temperature of the mixing layers was kept constant at 40°C for both light sources, we can also rule out thermally induced ordering. From the morphological analyses, we learned that UV-light introduces $PC_{71}BM$ migration into the polymer blend which increases the crystalline organization of fullerenes as well as the size of the acceptor domains. While annealing the cells already promotes both of these parameters, the presence of UV-light in the AM1.5 spectrum acts as a supplementary driving force for fullerene migration.

In the case of as-cast PTB7-Th:$PC_{71}BM$ blends where residual DIO molecules are present in the films, the dispersion solvent here CB is eliminated during the vacuum phase, while residual DIO molecules remain in the blend in trace amounts [37,38]. As previously mentioned, there is a photochemical reaction of $PC_{71}BM$ due to UV-induced DIO radicals, which leads to the formation of traps within the blend, increasing recombination and thus reducing device performance by triggering burn-in [25,45]. For this reason, one would expect a continued decline in PCE. Nevertheless, after this initial and long burn-in (zone I in Figure 2), as-cast devices show an unexpected behavior for PCE and FF parameters with a self-healing effect leading to stable solar cells under UV-light soaking (zone II in Figure 2). This observation highlights a second DIO-assisted process that will introduce a trend reversal. Therefore, the presence of residual DIO molecules may also have a beneficial effect. Due to the higher solubility of fullerene in DIO compared to the polymer [20, 21], the DIO molecules are located in close proximity to the fullerenes and thus increase the mobility of $PC_{71}BM$. Such a diffusion process may participate to the self-healing effect under UV-light in as-cast devices by enlargement and crystallization of fullerene domains (see Figure 4). The initial negative effect of DIO is counteracted by this second process to achieve a long lifetime (zone II in Figure 2). This improvement in UV stability due to increased crystallinity within the blend, especially in the $PC_{71}BM$ domains, was also observe by Liu *et al.* for inverted devices using DIO processed PTB7-Th:$PC_{71}BM$ blends [21].

Based on our previous work, we can state that the PAS-140 annealed thin films are instead free of DIO [31]. In this particular situation of absence of residual DIO molecules, neither an accentuated burn-in nor a degradation is observed. On the contrary, high stability is maintained over a long period of UV-containing light soaking. The results clearly show that a thermal annealing step applied to fresh layers spontaneously improves the UV stability of normal solar cells (zone I of PAS-140 in Figure 2), confirming that improved crystallization of fullerenes reduces the UV light degradation [21]. In addition, the post-annealing generates larger crystalline

domains of fullerenes that were even slowly strengthened during photoaging, which explains the high regularity of the FF value of PAS-140 aged devices.

These subtle changes in the nanomorphology of blends correlated well with the observed UV-stability of performances, which supported the hypothesis that the most important factor affecting the long-term stability under UV-light of solar cells is the ability of fullerenes to reorganize into large ordered assemblies.

4. Conclusion

The improvement of stability of polymer solar cells under AM1.5 illumination is one of the most important challenges for their commercialization. In this work the stability of solar cell in normal device structure using a well-known polymer blend based on PTB7-Th and $PC_{71}BM$ processed with DIO as additive were studied under continuous illumination with either a UV-containing simulated AM1.5 light or a UV-free LED light. PAS-140 post-annealed devices, resulting in DIO-free blends, show a high UV-stability without losses over more than 250 h. In contrast, with residual DIO incorporated into the blend, as-cast devices show an initial loss of performance, followed by a self-healing process leading to performance recovery and, more importantly, high UV-stability. Two DIO-assisted processes under UV-light have been involved: (i) creation of trap states and (ii) increased mobility of $PC_{71}BM$ molecules. The second one takes over from the first one to enhance the reorganization of the fullerenes leading to an improvement of the crystallinity and the size of the $PC_{71}BM$ domains. Overall, we have shown here that UV-light assisted crystallization of fullerenes occurs in BHJs, leading to larger and better ordered fullerene domains, thereby making a favourable stabilization of OSCs.

AUTHOR INFORMATION

Corresponding Authors
* E-mail: *christine.videlot-ackermann@cnrs.fr* (Christine Videlot-Ackermann)

ORCID
Anass Khor: 0000-0002-8521-7641
Sadok Ben Dkhil: 0000-0002-8035-7581
Pavlo Perkhun: 0000-0001-7458-3411
Yatzil Alejandra Avalos Quiroz: 0000-0002-8083-0527
Tomoyuki Koganezawa 0000-0002-9302-5025
Martin Pfammöler: 0000-0002-0910-1591
Olivier Margeat: 0000-0003-3716-2399
Jörg Ackermann: 0000-0003-2586-3788
Christine Videlot-Ackermann: 0000-0001-8240-6474

Author Contributions
The manuscript was written through contributions of all authors. All authors have given approval to the final version of the manuscript.

Notes
The authors declare no competing financial interest.

Acknowledgments
This work has been carried out within the framework of a CIFRE PhD grant 2017/0529 to E.B. from the ANRT (Association Nationale de la Recherche et de la Technologie) and the Ministère de l'Enseignement Supérieur, de la Recherche et de l'Innovation, awarded through the company Dracula Technologies (Valence, France). P.P. and J.A. received funding from the European Union's Horizon 2020 research and innovation program under the Marie Skłodowska-Curie Grant Agreement No. 713750. They further acknowledge support of the Regional Council of Provence-Alpes-Côte d'Azur, A*MIDEX (No. ANR-11-IDEX-0001-02), and the Investissements d'Avenir project funded by the French Government, managed by the French National Research Agency (ANR). This project has also received funding by the French Research Agency (project ANR-17-CE05-0020-01 named NFA-15). The synchrotron radiation experiments were performed at BL19B2 in SPring-8 with the approval of Japan Synchrotron Radiation Research Institute (JASRI) (Proposal Nos. 2018B1791 and 2019B1851).

References

[1] Y. Cui, H. Yao, J. Zhang, K. Xian, T. Zhang, L. Hong, Y. Wang, Y. Xu, K. Ma, C. An, C. He, Z. Wei, F. Gao, J. Hou, Single- Junction Organic Photovoltaic Cells with Approaching 18% Efficiency, Adv. Mater. 32 (2020) 1908205. https://doi.org/10.1002/adma.201908205.
[2] S. Li, L. Zhan, Y. Jin, G. Zhou, T. Lau, R. Qin, M. Shi, C. Li, H. Zhu, X. Lu, F. Zhang, H. Chen, Asymmetric Electron Acceptors for High- Efficiency and Low- Energy- Loss Organic Photovoltaics, Adv. Mater. 32 (2020) 2001160. https://doi.org/10.1002/adma.202001160.
[3] Q. Liu, Y. Jiang, K. Jin, J. Qin, J. Xu, W. Li, J. Xiong, J. Liu, Z. Xiao, K. Sun, S. Yang,

X. Zhang, L. Ding, 18% Efficiency organic solar cells, Sci. Bull. 65 (2020) 272–275. https://doi.org/10.1016/j.scib.2020.01.001.
[4] D. Dang, D. Yu, E. Wang, Conjugated Donor–Acceptor Terpolymers Toward High- Efficiency Polymer Solar Cells, Adv. Mater. 31 (2019) 1807019. https://doi.org/10.1002/adma.201807019.
[5] L. Zhan, S. Li, T.-K. Lau, Y. Cui, X. Lu, M. Shi, C.-Z. Li, H. Li, J. Hou, H. Chen, Over 17% efficiency ternary organic solar cells enabled by two non-fullerene acceptors working in an alloy-like model, Energy Environ. Sci. 13 (2020) 635–645. https://doi.org/10.1039/C9EE03710A.
[6] L. Liu, Y. Kan, K. Gao, J. Wang, M. Zhao, H. Chen, C. Zhao, T. Jiu, A. - Y. Jen, Y. Li, Graphdiyne Derivative as Multifunctional Solid Additive in Binary Organic Solar Cells with 17.3% Efficiency and High Reproductivity, Adv. Mater. 32 (2020) 1907604. https://doi.org/10.1002/adma.201907604.
[7] F. Zhao, H. Zhang, R. Zhang, J. Yuan, D. He, Y. Zou, F. Gao, Emerging Approaches in Enhancing the Efficiency and Stability in Non- Fullerene Organic Solar Cells, Adv. Energy Mater. 10 (2020) 2002746. https://doi.org/10.1002/aenm.202002746.
[8] L. Ye, H. Hu, M. Ghasemi, T. Wang, B.A. Collins, J.-H. Kim, K. Jiang, J.H. Carpenter, H. Li, Z. Li, T. McAfee, J. Zhao, X. Chen, J.L.Y. Lai, T. Ma, J.-L. Bredas, H. Yan, H. Ade, Quantitative relations between interaction parameter, miscibility and function in organic solar cells, Nat. Mater. 17 (2018) 253–260. https://doi.org/10.1038/s41563-017-0005-1.
[9] D. Deng, Y. Zhang, J. Zhang, Z. Wang, L. Zhu, J. Fang, B. Xia, Z. Wang, K. Lu, W. Ma, Z. Wei, Fluorination-enabled optimal morphology leads to over 11% efficiency for inverted small-molecule organic solar cells, Nat. Commun. 7 (2016) 13740. https://doi.org/10.1038/ncomms13740.
[10] D. Baran, R.S. Ashraf, D.A. Hanifi, M. Abdelsamie, N. Gasparini, J.A. Röhr, S. Holliday, A. Wadsworth, S. Lockett, M. Neophytou, C.J.M. Emmott, J. Nelson, C.J. Brabec, A. Amassian, A. Salleo, T. Kirchartz, J.R. Durrant, I. McCulloch, Reducing the efficiency–stability–cost gap of organic photovoltaics with highly efficient and stable small molecule acceptor ternary solar cells, Nat. Mater. 16 (2017) 363–369. https://doi.org/10.1038/nmat4797.
[11] B. Fan, X. Du, F. Liu, W. Zhong, L. Ying, R. Xie, X. Tang, K. An, J. Xin, N. Li, W. Ma, C.J. Brabec, F. Huang, Y. Cao, Fine-tuning of the chemical structure of photoactive materials for highly efficient organic photovoltaics, Nat. Energy. 3 (2018) 1051–1058. https://doi.org/10.1038/s41560-018-0263-4.
[12] S.M. Menke, N.A. Ran, G.C. Bazan, R.H. Friend, Understanding Energy Loss in Organic Solar Cells: Toward a New Efficiency Regime, Joule. 2 (2018) 25–35. https://doi.org/10.1016/j.joule.2017.09.020.
[13] Z. Zhou, S. Xu, J. Song, Y. Jin, Q. Yue, Y. Qian, F. Liu, F. Zhang, X. Zhu, High-efficiency small-molecule ternary solar cells with a hierarchical morphology enabled by synergizing fullerene and non-fullerene acceptors, Nat. Energy. 3 (2018) 952–959. https://doi.org/10.1038/s41560-018-0234-9.
[14] K. Gao, S.B. Jo, X. Shi, L. Nian, M. Zhang, Y. Kan, F. Lin, B. Kan, B. Xu, Q. Rong, L. Shui, F. Liu, X. Peng, G. Zhou, Y. Cao, A.K. - Y. Jen, Over 12% Efficiency Nonfullerene All- Small- Molecule Organic Solar Cells with Sequentially Evolved Multilength Scale Morphologies, Adv. Mater. 31 (2019) 1807842. https://doi.org/10.1002/adma.201807842.
[15] S.B. Sapkota, M. Fischer, B. Zimmermann, U. Würfel, Analysis of the degradation mechanism of ITO-free organic solar cells under UV radiation, Sol. Energy Mater. Sol.

Cells. 121 (2014) 43–48.
https://doi.org/10.1016/j.solmat.2013.10.021.
[16] T. Leijtens, G.E. Eperon, S. Pathak, A. Abate, M.M. Lee, H.J. Snaith, Overcoming ultraviolet light instability of sensitized TiO2 with meso-superstructured organometal tri-halide perovskite solar cells, Nat. Commun. 4 (2013) 2885.
https://doi.org/10.1038/ncomms3885.
[17] A. Uddin, M. Upama, H. Yi, L. Duan, Encapsulation of Organic and Perovskite Solar Cells: A Review, Coatings. 9 (2019) 65.
https://doi.org/10.3390/coatings9020065.
[18] S. Ben Dkhil, P. Perkhun, C. Luo, D. Müller, R. Alkarsifi, E. Barulina, Y.A. Avalos Quiroz, O. Margeat, S.T. Dubas, T. Koganezawa, D. Kuzuhara, N. Yoshimoto, C. Caddeo, A. Mattoni, B. Zimmermann, U. Würfel, M. Pfannmöller, S. Bals, J. Ackermann, C. Videlot-Ackermann, Direct Correlation of Nanoscale Morphology and Device Performance to Study Photocurrent Generation in Donor-Enriched Phases of Polymer Solar Cells, ACS Appl. Mater. Interfaces. 12 (2020) 28404–28415.
https://doi.org/10.1021/acsami.0c05884.
[19] M. Prosa, M. Tessarolo, M. Bolognesi, O. Margeat, D. Gedefaw, M. Gaceur, C. Videlot-Ackermann, M.R. Andersson, M. Muccini, M. Seri, J. Ackermann, Enhanced Ultraviolet Stability of Air-Processed Polymer Solar Cells by Al Doping of the ZnO Interlayer, ACS Appl. Mater. Interfaces. 8 (2016) 1635–1643.
https://doi.org/10.1021/acsami.5b08255.
[20] J. Jeong, J. Seo, S. Nam, H. Han, H. Kim, T.D. Anthopoulos, D.D.C. Bradley, Y. Kim, Significant Stability Enhancement in High- Efficiency Polymer:Fullerene Bulk Heterojunction Solar Cells by Blocking Ultraviolet Photons from Solar Light, Adv. Sci. 3 (2016) 1500269.
https://doi.org/10.1002/advs.201500269.
[21] Q. Liu, J. Toudert, F. Liu, P. Mantilla- Perez, M.M. Bajo, T.P. Russell, J. Martorell, Circumventing UV Light Induced Nanomorphology Disorder to Achieve Long Lifetime PTB7- Th:PCBM Based Solar Cells, Adv. Energy Mater. 7 (2017) 1701201.
https://doi.org/10.1002/aenm.201701201.
[22] W.R. Mateker, M.D. McGehee, Progress in Understanding Degradation Mechanisms and Improving Stability in Organic Photovoltaics, Adv. Mater. 29 (2017) 1603940.
https://doi.org/10.1002/adma.201603940.
[23] B.A. MacLeod, B.J. Tremolet de Villers, P. Schulz, P.F. Ndione, H. Kim, A.J. Giordano, K. Zhu, S.R. Marder, S. Graham, J.J. Berry, A. Kahn, D.C. Olson, Stability of inverted organic solar cells with ZnO contact layers deposited from precursor solutions, Energy Environ. Sci. 8 (2015) 592–601.
https://doi.org/10.1039/C4EE02488E.
[24] Y. Wang, M.J. Jafari, N. Wang, D. Qian, F. Zhang, T. Ederth, E. Moons, J. Wang, O. Inganäs, W. Huang, F. Gao, Light-induced degradation of fullerenes in organic solar cells: a case study on TQ1:PC 71 BM, J. Mater. Chem. A. 6 (2018) 11884–11889.
https://doi.org/10.1039/C8TA03112F.
[25] A. Classen, T. Heumueller, I. Wabra, J. Gerner, Y. He, L. Einsiedler, N. Li, G.J. Matt, A. Osvet, X. Du, A. Hirsch, C.J. Brabec, Revealing Hidden UV Instabilities in Organic Solar Cells by Correlating Device and Material Stability, Adv. Energy Mater. 9 (2019) 1902124. https://doi.org/10.1002/aenm.201902124.
[26] M. Qin, P. Cheng, J. Mai, T.-K. Lau, Q. Zhang, J. Wang, C. Yan, K. Liu, C.-J. Su, W. You, X. Lu, X. Zhan, Enhancing Efficiency and Stability of Organic Solar Cells by UV Absorbent, Sol. RRL. 1 (2017) 1700148.
https://doi.org/10.1002/solr.201700148.

[27] A.J. Pearson, P.E. Hopkinson, E. Couderc, K. Domanski, M. Abdi-Jalebi, N.C. Greenham, Critical light instability in CB/DIO processed PBDTTT-EFT:PC 71 BM organic photovoltaic devices, Org. Electron. 30 (2016) 225–236. https://doi.org/10.1016/j.orgel.2015.12.024.
[28] W. Kim, J.K. Kim, E. Kim, T.K. Ahn, D.H. Wang, J.H. Park, Conflicted Effects of a Solvent Additive on PTB7:PC 71 BM Bulk Heterojunction Solar Cells, J. Phys. Chem. C. 119 (2015) 5954–5961. https://doi.org/10.1021/jp510996w.
[29] N.Y. Doumon, G. Wang, R.C. Chiechi, L.J.A. Koster, Relating polymer chemical structure to the stability of polymer:fullerene solar cells, J. Mater. Chem. C. 5 (2017) 6611–6619. https://doi.org/10.1039/C7TC01455D.
[30] S. Ben Dkhil, M. Pfannmöller, R.R. Schröder, R. Alkarsifi, M. Gaceur, W. Köntges, H. Heidari, S. Bals, O. Margeat, J. Ackermann, C. Videlot-Ackermann, Interplay of Interfacial Layers and Blend Composition To Reduce Thermal Degradation of Polymer Solar Cells at High Temperature, ACS Appl. Mater. Interfaces. 10 (2018) 3874–3884. https://doi.org/10.1021/acsami.7b17021.
[31] S. Ben Dkhil, M. Pfannmöller, M.I. Saba, M. Gaceur, H. Heidari, C. Videlot-Ackermann, O. Margeat, A. Guerrero, J. Bisquert, G. Garcia-Belmonte, A. Mattoni, S. Bals, J. Ackermann, Toward High-Temperature Stability of PTB7-Based Bulk Heterojunction Solar Cells: Impact of Fullerene Size and Solvent Additive, Adv. Energy Mater. 7 (2017) 1601486. https://doi.org/10.1002/aenm.201601486.
[32] T.S. Yoo, M.J. Ackerman, W.E. Lorensen, W. Schroeder, V. Chalana, S. Aylward, D. Metaxas, R. Whitaker, Engineering and Algorithm Design for an Image Processing[API: A Technical Report on ITK - The Insight Toolkit, in: Med. Meets Virtual Real. 02/10 - Digit. Upgrad. Appl. Moore's Law to Heal. IOS Press, n.d.: pp. 586–592. https://doi.org/10.3233/978-1-60750-929-5-586.
[33] C. Sommer, C. Straehle, U. Kothe, F.A. Hamprecht, Ilastik: Interactive learning and segmentation toolkit, in: 2011 IEEE Int. Symp. Biomed. Imaging From Nano to Macro, IEEE, Chicago, IL, USA, 2011: pp. 230–233. https://doi.org/10.1109/ISBI.2011.5872394.
[34] M. Pfannmöller, H. Flügge, G. Benner, I. Wacker, C. Sommer, M. Hanselmann, S. Schmale, H. Schmidt, F.A. Hamprecht, T. Rabe, W. Kowalsky, R.R. Schröder, Visualizing a Homogeneous Blend in Bulk Heterojunction Polymer Solar Cells by Analytical Electron Microscopy, Nano Lett. 11 (2011) 3099–3107. https://doi.org/10.1021/nl201078t.
[35] W. Köntges, P. Perkhun, J. Kammerer, R. Alkarsifi, U. Würfel, O. Margeat, C. Videlot-Ackermann, J.-J. Simon, R.R. Schröder, J. Ackermann, M. Pfannmöller, Visualizing morphological principles for efficient photocurrent generation in organic non-fullerene acceptor blends, Energy Environ. Sci. 13 (2020) 1259–1268. https://doi.org/10.1039/C9EE03535D.
[36] R.F. Egerton, Electron Energy-Loss Spectroscopy in the Electron Microscope, Third Ed Springer US, Boston, MA, 2011.
[37] I.E. Jacobs, F. Wang, Z.I. Bedolla Valdez, A.N. Ayala Oviedo, D.J. Bilsky, A.J. Moulé, Photoinduced degradation from trace 1,8-diiodooctane in organic photovoltaics, J. Mater. Chem. C. 6 (2018) 219–225. https://doi.org/10.1039/C7TC04358A.
[38] H. Waters, N. Bristow, O. Moudam, S.-W. Chang, C.-J. Su, W.-R. Wu, U.-S. Jeng, M. Horie, J. Kettle, Effect of processing additive 1,8-octanedithiol on the lifetime of

PCPDTBT based Organic Photovoltaics, Org. Electron. 15 (2014) 2433–2438. https://doi.org/10.1016/j.orgel.2014.06.031.
[39] C. McDowell, M. Abdelsamie, M.F. Toney, G.C. Bazan, Solvent Additives: Key Morphology-Directing Agents for Solution-Processed Organic Solar Cells, Adv. Mater. 30 (2018) 1707114. https://doi.org/10.1002/adma.201707114.
[40] S.B. Dkhil, M. Pfannmöller, M.I. Saba, M. Gaceur, H. Heidari, C. Videlot- Ackermann, O. Margeat, A. Guerrero, J. Bisquert, G. Garcia- Belmonte, A. Mattoni, S. Bals, J. Ackermann, Toward High-Temperature Stability of PTB7-Based Bulk Heterojunction Solar Cells: Impact of Fullerene Size and Solvent Additive, Adv. Energy Mater. 7 (2017) 1601486. https://doi.org/10.1002/aenm.201601486.
[41] H. Lu, B. Akgun, T.P. Russell, Morphological Characterization of a Low-Bandgap Crystalline Polymer:PCBM Bulk Heterojunction Solar Cells, Adv. Energy Mater. 1 (2011) 870–878. https://doi.org/10.1002/aenm.201100128.
[42] Q. Sun, F. Zhang, J. Wang, Q. An, C. Zhao, L. Li, F. Teng, B. Hu, A two-step strategy to clarify the roles of a solution processed PFN interfacial layer in highly efficient polymer solar cells, J. Mater. Chem. A. 3 (2015) 18432–18441. https://doi.org/10.1039/C5TA05117G.
[43] C. Lindqvist, A. Sanz-Velasco, E. Wang, O. Bäcke, S. Gustafsson, E. Olsson, M.R. Andersson, C. Müller, Nucleation-limited fullerene crystallisation in a polymer–fullerene bulk-heterojunction blend, J. Mater. Chem. A. 1 (2013) 7174. https://doi.org/10.1039/c3ta11018d.
[44] E. Verploegen, R. Mondal, C.J. Bettinger, S. Sok, M.F. Toney, Z. Bao, Effects of Thermal Annealing Upon the Morphology of Polymer-Fullerene Blends, Adv. Funct. Mater. 20 (2010) 3519–3529. https://doi.org/10.1002/adfm.201000975.
[45] H. Zhang, T. Stubhan, N. Li, M. Turbiez, G.J. Matt, T. Ameri, C.J. Brabec, A solution-processed barium hydroxide modified aluminum doped zinc oxide layer for highly efficient inverted organic solar cells, J. Mater. Chem. A. 2 (2014) 18917–18923. https://doi.org/10.1039/C4TA03421J.